NREL/SR-520-21928 • UC Category: 1262 • DE96014326

Experimental Study of the Factors Governing the Staebler-Wronski Photodegradation Effect in a-Si:H Solar Cells

Annual Subcontract Report
1 April 1995 - 30 June 1996

D. Han
University of North Carolina
Chapel Hill, North Carolina

NREL technical monitor: B. von Roedern

National Renewable Energy Laboratory
1617 Cole Boulevard
Golden, Colorado 80401-3393
A national laboratory of
the U.S. Department of Energy
Managed by Midwest Research Institute
for the U.S. Department of Energy
under Contract No. DE-AC36-83CH10093

Prepared under Subcontract No. XAN-4-13318-09
October 1996

Available to DOE and DOE contractors from:
Office of Scientific and Technical Information (OSTI)
P.O. Box 62
Oak Ridge, TN 37831
Prices available by calling (423) 576-8401

Available to the public from:
National Technical Information Service (NTIS)
U.S. Department of Commerce
5285 Port Royal Road
Springfield, VA 22161
(703) 487-4650

Printed on paper containing at least 50% wastepaper, including 20% postconsumer waste

PREFACE

This report covers the work performed by UNC-CH for the period April 1, 1995 to June 30, 1996 under subcontract No. XAN-4-13318-09.

The following personnel participated in the research program. Daxing Han (P.I.), Keda Wang, and C. N. Yeh. We have also benefited from numerous discussions and cooperation with our Condensed Matter colleagues at UNC-CH, Prof. L. E. McNeil, Prof. Y. Wu, Mr. T. J. Stephen. At other institutions we have collaborated with G. J. Adriaessens, B. Yan at K. University Leuven, Belgium, L.Y Yang at Solarex, and mostly with R. Crandall, Qi Wang, and H. Mahan at NREL.

The samples were obtained from Team members, L. Y. Yang, Y. M. Li at Solarex, X. M. Deng at Energy Conversion Devices (ECD), S. Hegedus at Institute for Energy Conversion (IEC) at Delaware, and R. Crandall and H. Mahan at National Renewable Energy Laboratory (NREL).

TABLE OF CONTENTS

LIST OF FIGURES

SUMMARY

Our goal is to help the U. S. amorphous silicon PV industry to achieve the U.S./DOE PV Program milestone of 12% stable efficiency modules by 1998.

We have concentrated on determining the factors controlling the SWE in a-Si:H p-i-n solar cells, and on the correlation of the material properties to the cell preparation conditions such as the effect of hydrogen-dilution.

During the contract year, April 1, 1995 - June 30, 1996, the a-Si:H p-i-n solar cells made with and without hydrogen-dilution at Solarex were systematically studied by electroluminescence (EL) measurements; we have started the internal electric field profile $E_i(x)$ measurements in p-i-n structures by a null-current method; we studied DOS profile in p-i-n devices; and the hydrogen distribution in hot-wire a-Si:H films are being studied by nuclear magnetic resonance (NMR).

The a-Si:H material photoelectric properties have been characterized by $\mu\tau$ product and the density of defect states (DOS). Unfortunately, these parameters do not correlate well with cell performance. We have developed electroluminescence (EL) spectroscopy to measure the defect energy profile and to characterize SWE in real solar cell structures, and to correlate with the cell performance as well. The temperature and applied voltage dependence of both the EL efficiency and the EL energy spectrum were investigated before and after light soaking, and the results will be given in section I. We found that the hydrogen-dilution modifies the localized state distribution in the i-layer, especially to narrow the defect energy distribution and then to improve the cell performance.

Section II shows the results of DOS by comparison studies of post-transient-photocurrent and EL spectroscopy.

In section III we present our results of electric field profiling studies in p-i-n structures.

Section IV explores the microstructure origin which leads to more stable new a-Si:H materials. We have carried out proton NMR and Multiple-Quantum NMR studies on hot-wire samples. The results show the hydrogen distribution on hot-wire samples.

Our research last year has resulted in nine publications, one to be published and one submitted paper, and the submission of five quarterly reports, one final subcontract report, one annual technical report, and reports for the team meetings.

INTRODUCTION

This report describes the research performed during Phase II of a three-phase, three year project under NREL Subcontract No. XAN-4-13318-09.

One of the biggest problems for the widespread use of hydrogenated amorphous silicon (a-Si:H) based solar cells is the so-called Staebler-Wronski effect (SWE).[1] This reversible light-induced degradation of the photovoltaic properties has been the focus of intense research for well over a decade. Up to now, the understanding of the metastable changes in the defect states in terms of their physical mechanism, the kinetics, the linkage with the atomic microstructure etc., is still poor.[2] This is especially true in device structures. However, most agree[2,3] that: (1) an increase of the total density of neutral dangling bonds (DB), that is observed to often scale inversely with the carrier mobility-lifetime product $\mu\tau$; (2) hydrogen is involved in some way. The questions are (1) why do the kinetics of the photodegradation show "fast" and a "slow" defects[4,5] in solar cells? and (2) what is the linkage between hydrogen microstructure and metastability? This information is lacking. Understanding these linkages would be an important ingredient in understanding the actual degradation mechanism.

The purpose of our research is to address the above questions through studies of EL, electric field profiles on p-i-n solar cells, and of the proton NMR on new materials.

1) Electroluminescence (EL)

EL is a result of carrier radiative recombination in the intrinsic-layer of the p-i-n solar cells. The emission photon energy depends on the carrier distribution in the localized states. By studying the EL spectra and their temperature dependence we can determine the energy distribution of both the tail states and defect states, while degradation of EL spectrum as a function of light-soaking time will reveal the kinetics.

2) Transient photocurrents (TPC)

TPC can probe both shallow and deep traps. Post-transit TPC is a tool to study the energy profile of defect states which is involved in the SWE.

3) Electronic Profiling

The electric field profile varies depending upon where recombination takes place. We have completed the equipment set-up and started the measurements in a-Si:H solar cells.

4) NMR

Since Si-H bonds play an important role in the metastability, we have studied local Si-H bonding configurations by NMR to find why the new hot-wire material does show better stability.

RESULTS

I. Electroluminescence (EL)

I.1 Introduction

The performance of a-Si:H solar cells is believed to be determined, to a large extent, by the density of gap states (DOS) in the intrinsic i-layer. Several techniques are available to characterize the DOS in a-Si:H films. However, the electronic parameters in the films, such as mobility-lifetime product, $\mu\tau$, and DOS obtained from constant photocurrent method (CPM) measurements do not correlate well with cell performance.[6] Therefore, a suitable technique to measure recombination and DOS in real solar cells is needed. EL spectroscopy measurements were carried out for this purpose.

Under forward bias, electrons and holes are injected into the i-layer from opposite sides of the diode. The steady state forward current is a recombination limited current. EL is the result of excess electron-hole radiative recombination in the i-layer. At low temperature, the tail-to-tail transition gives the main-band luminescence, EL_m. At room temperatures, the tail-to-defect radiative recombination gives the defect-band luminescence, EL_d. Since electron mobility-lifetime product is larger than the hole's, $\mu_n\tau_n >> \mu_p\tau_p$, the electron current dominates the forward current. The generation rate of EL, g, is defined as the number of injected electrons that recombine with holes per cm^3, per second. It can be expressed in terms of the density of forward bias current,[7]

$$g = J_F/eL(\tau/t_0) \cong J_FL/e\mu_n\tau_nV_i, \qquad (1.1)$$

where e is the charge of an electron, L is the thickness of the i-layer, $(\tau/t_0) = \mu\tau E/L \cong \mu_n\tau_nV_i$ is the gain factor, and V_i is the voltage across the i-layer. The EL quantum efficiency, I_{EL}/g, then can be expressed as

$$\eta_{EL} \cong \frac{I_{EL}}{J_F} \times e\mu_n\tau_nE. \qquad (1.2)$$

It is well known from photoluminescence (PL) studies[1] that at low temperature (T<100 K) the dominant recombination in a-Si:H is the radiative transition between band tail states. The efficiency of the tail-to-tail radiative recombination is thermally quenched as the temperature increases. In a simple thermal quenching model [8] with exponential tail states $g_o\exp(-E/kT_0)$, when the luminescence efficiency is $y_L<<1$, the temperature dependence of y_L is described by

$$y_L = y_0\exp(-E_D/kT_0) = y_0\exp(-T/T_L) \qquad (1.3)$$

where $E_D = kT\ln(\nu_0\tau_r)$ is a demarcation energy and the slope $T_L = T_0/\ln\nu_0\tau_r$. All states deeper than E_D will have a high probability of radiative recombination, whereas shallower states will be excited to the mobility edge and will diffuse away to a nonradiative center. A slope of 20 - 25 K in PL intensity vs. T curves was found and attributed to the width of the valence band tail $T_0 \approx$ 500 K by using an average lifetime $\tau_r \approx 10^{-3}$ s in a-Si:H films. In order to obtain the valence band tail slope from the luminescence thermalization processes, one must keep a constant generation rate. According to Eq. (1) the generation rate will be unchanged under constant voltage condition. A small thermal activation energy of $\mu_n\tau_n$ product can be taken into account later.

In PL at low temperatures, the radiative transition from the band tail to the defects, on the other hand, is 4 orders of magnitude weaker than the main-band luminescence with a weak temperature dependence. Hence, the defect PL band only has been observed in either high-defect or doped materials at low temperatures.[9] Generally, at room temperature the PL efficiency is reduced by about four orders of magnitude compared to the value at 50 K and is barely detectable in intrinsic a-Si:H samples. We will see that the advantage of EL is the relatively strong defect luminescence signal that allows us to study the defect energy profile at room temperature.

Yang and Chen at Solarex found that "fast" and "slow" defects co-exit in solar cells made with pure silane; cells made with H-dilution appear to have a great predominance of "fast" defects, resulting in a much faster saturation of photodegradation.[4,5] Several laboratories report that the a-Si:H solar cells with H-dilution have better performance after light-soaking than those without H-dilution. To understand the role of hydrogen-dilution in metastability, the carrier recombination process and the nature of localized states are crucial. We use EL spectroscopy to measure the energy profile of the localized states and their photodegradation kinetics in a-Si:H solar cells made with and without H-dilution.

I.2 Samples and experimental conditions

a-Si:H p-i-n solar cells were made by d.c. glow discharge by the team members at Solarex.[4,5] The 5,000 Å thick intrinsic layer material in the solar cells was made of either hydrogen-diluted silane or pure silane, denoted as p-i_H-n and p-i-n, respectively. The sample preparation conditions and cell performance are listed in Table I. The substrate surface was textured to avoid interference fringes. The top contacts were Al, andthe area was 0.1 to 0.3 cm^2. The two types of cells studied have similar initial energy conversion efficiencies, but under AM1.5 light soaking the p-i_H-n cells stabilized after about 100 h while the p-i-n cells did not stablize until after 1000 h.[4,5] Several cells were measured for each type of device to ensure good reproducibility.

For J_F and EL measurements, a micro-refrigerator stage was used to maintain the cell in the temperature range of 80 K to 350 K. The applied voltage was obtained from a programmable pulse generator. 10 Hz repetition rate and 10 ms pulse width were typically used. The Lock-in technique was used to collect the EL signal. The contribution of thermal radiation to the signal was less than 2% of the total signal. The emitted photons were dispersed in a monochromator and detected by a liquid-nitrogen-cooled Ge detector. The response curve of the detector and the system optics was calibrated by using a linear response detector. A scheme of the EL set-up is shown in Fig.1. A sample stage is described in Fig. 2. To minimum the tray resistance/ capacitance a Ohmic contact is needed for both EL and transient measurements. More detail about the experimental conditions can be found elsewhere.[10-14,16]

Table I Sample Preparation Conditions and Cell Performance

Cell I.D.	Thickness (Å)	Structure	Mode of Deposition	V_{oc} (volt)	J_{sc} (mA/cm^2)	Fill Factor	Efficiency %
SLX-1c	5,000	p-i_H-n	H-dilution	0.888	14.3	0.686	8.7
SLX-2c	5,000	p-i-n	pure silane	0.862	14.2	0.684	8.4

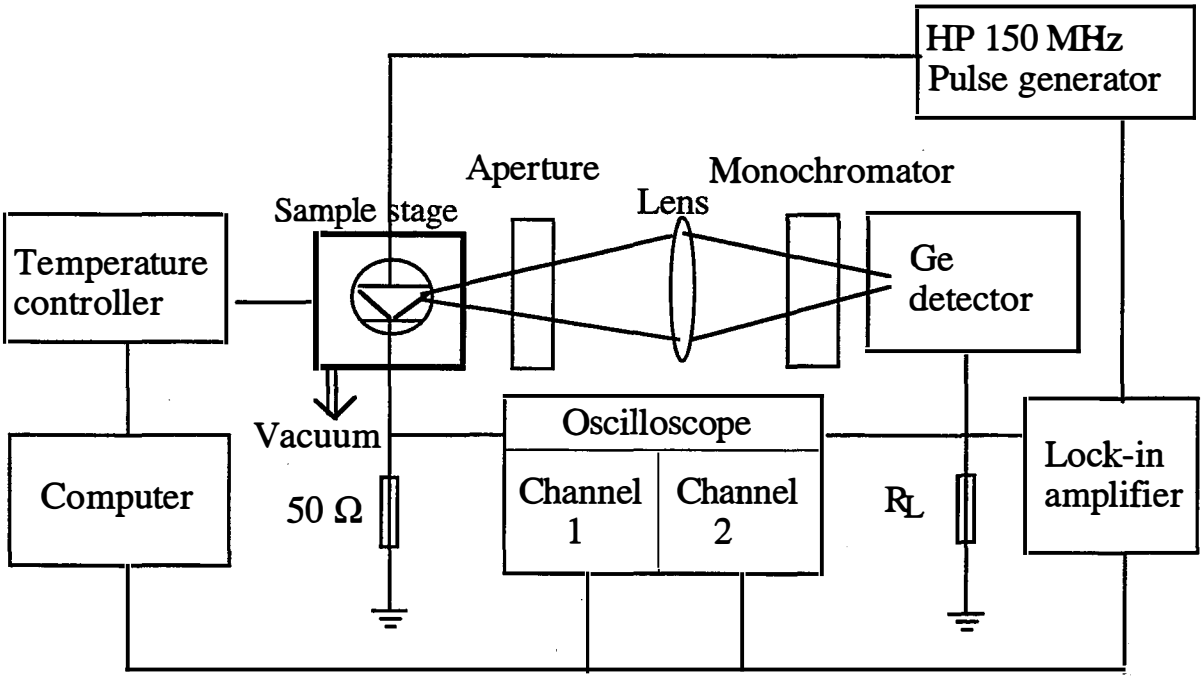

Fig. 1 EL Experimental Layout

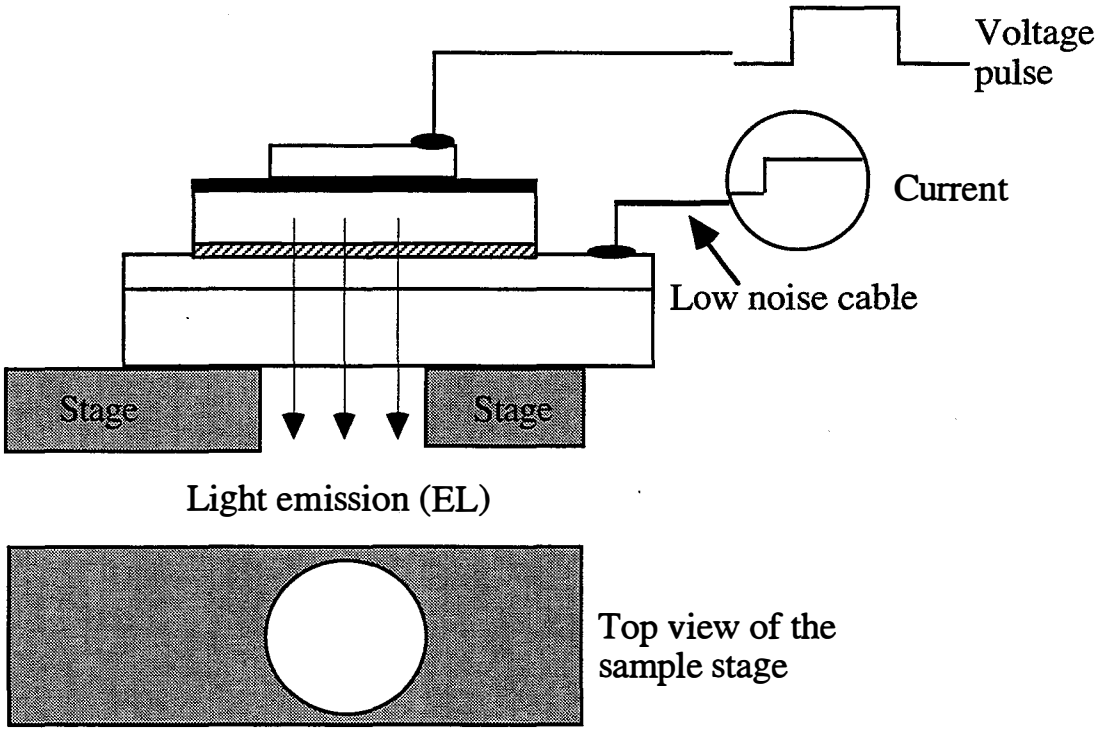

Fig. 2 Scheme of the EL experimental sample stage

I.3 EL results

EL efficiency temperature dependence of p-i_H-n and p-i-n cells

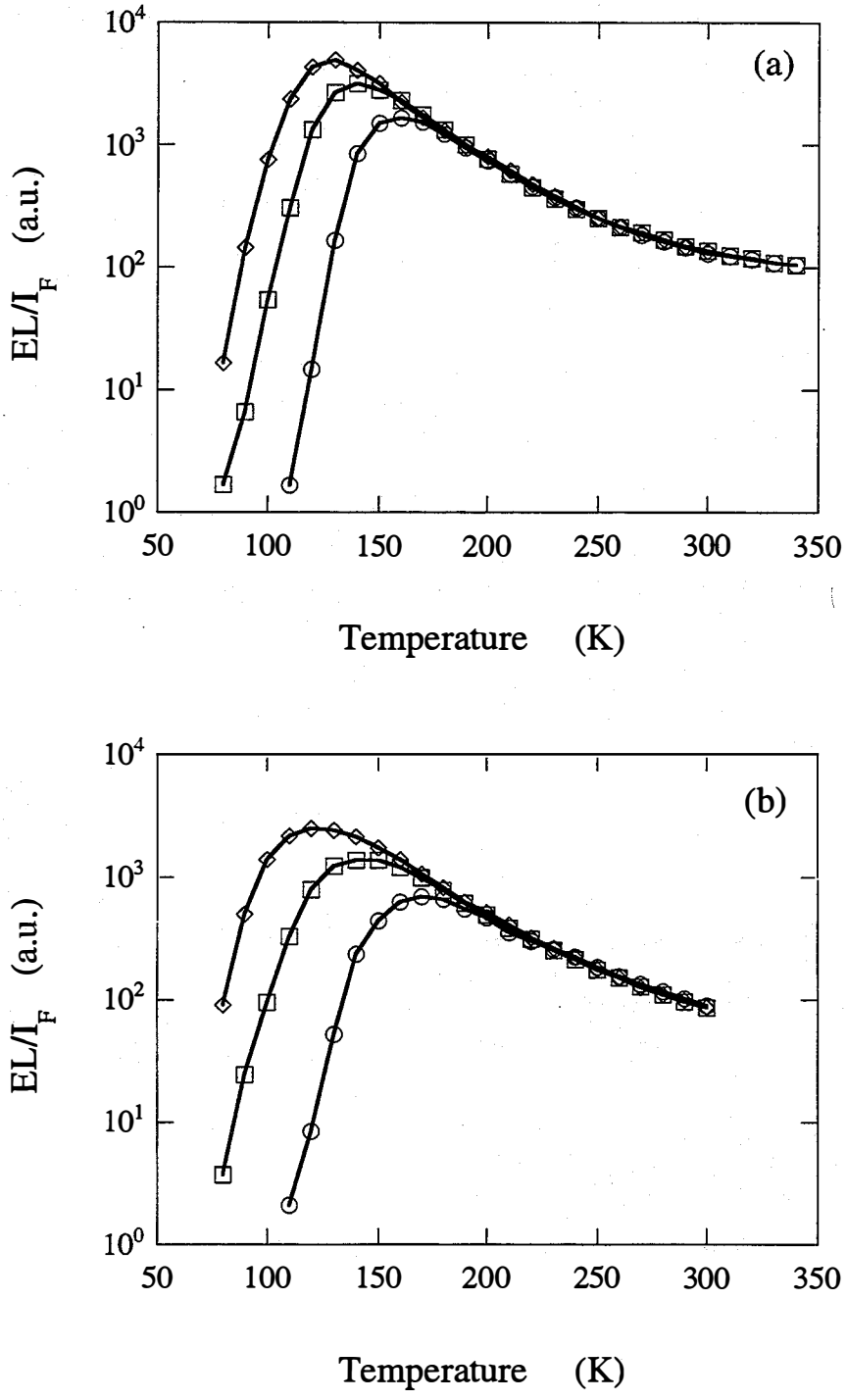

Fig. 3 Temperature dependence of effective EL efficiency, EL/J_F, under 2V, 3V and 4V for 0.5 μm thick a-Si:H (a) p-i_H-n, and (b) p-i-n cells.

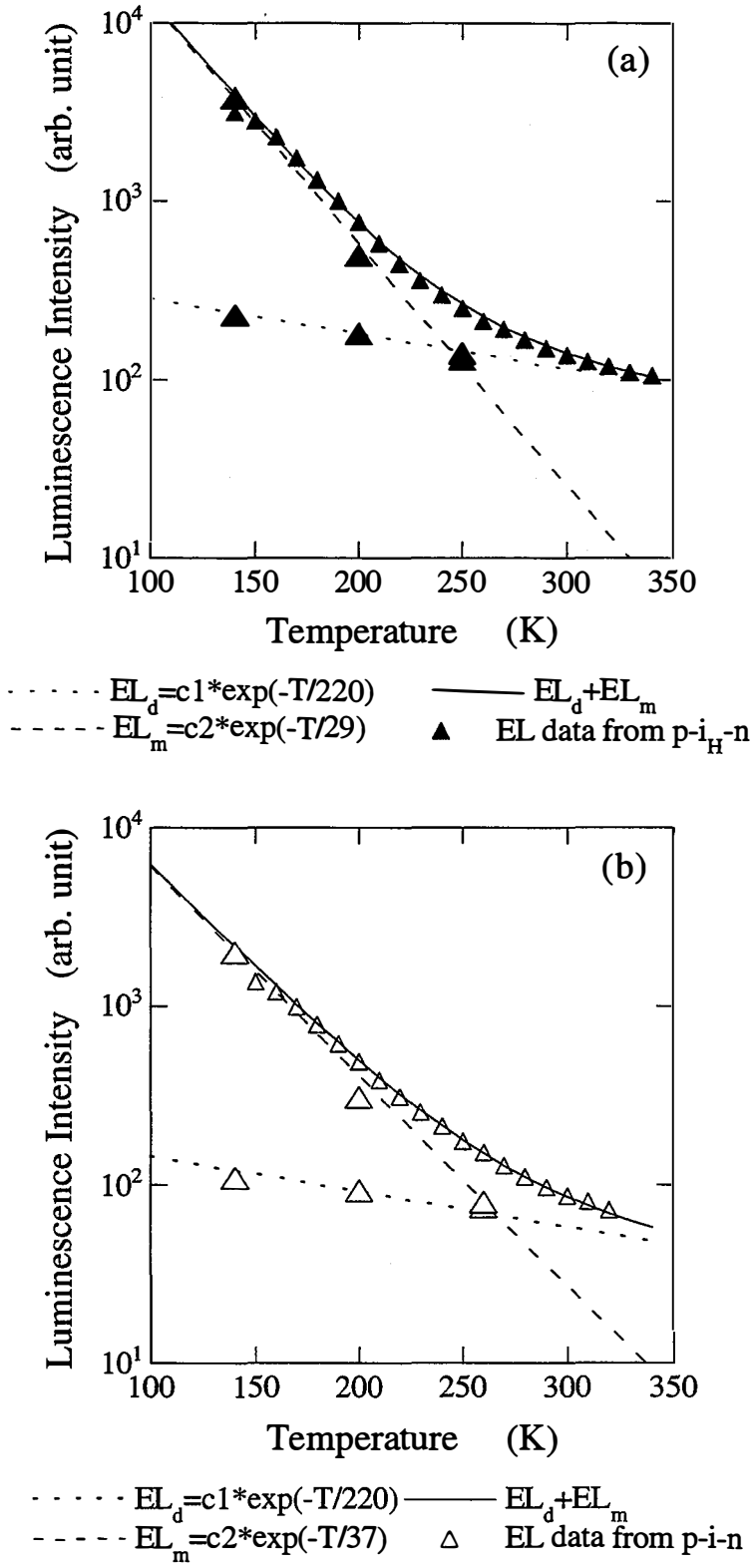

Fig. 4 The I_{EL}/I_F vs. T curve above 160 K for (a) p-i_H-n, and (b) p-i-n cells. The solid and open triangles are the measured data, EL_m and EL_d data were obtained by spectrum deconvolution.

The temperature dependence of the EL efficiency, EL/I_F under applied voltages of 2V, 3V and 4V are shown in Figs 3a and 3b for the p-i_H-n and p-i-n cells, respectively. The EL and I_F are the total emission and total current measured in the unit of mV and mA, respectively. So the sample area factor was canceled out. One can see that there is a maximum of EL/I_F at 130, 140, and 160 K in the p-i_H-n cell, and 120, 150, and 170 K in the p-i-n cell under 2, 3, and 4 V applied voltage, and then decreases somewhat exponentially as the temperature increases. We will not discuss the low temperature region but concentrate on the middle region in which we can obtain information of the localized states in the i-layer. In Figs. 4a and 4b the EL/I_F vs. T data above 160 K are re-plotted, and the contributions from both the main band EL_m and defect band EL_d are indicated for the p-i_H-n and p-i-n cells, respectively. The symbols of the solid and open triangles are the measured data from the p-i_H-n and p-i-n cells. EL_m and EL_d data were obtained by spectrum deconvolution at 140 K, 200 K, and 250 K.[10] The dotted and solid lines show the best fit by using the functions expressed under the Figures. First, one can see that the slope of the EL main band EL_m vs. T curve is deeper with T_L = 29 K in the p-i_H-n than that of T_L = 37 K in the p-i-n cell. This indicates a narrower valence band tail in the p-i_H-n than that in the p-i-n cell according to Eq. (1.3). Second, the EL defect band EL_d shows the same weak temperature dependence in both cells, but the relative intensity of the EL_d to EL_m is higher in the p-i_H-n cell. It could be due to more radiative recombination via the defect states in the H-diluted p-i_H-n cell than that in the non-diluted p-i-n cell. Because the dangling bond states act as either a non-radiative or a radiative recombination center depends on the environment. The detail mechanism needs to be studied.

EL intensity as a function of forward current density

Another way to study the recombination mechanism is to measure the EL efficiency as a function of the generation rate. As shown in Eq. (1.1), the generation rate of EL is related to the carrier transport in a manner of $g = J_F L/(e\mu\tau E)$.[7] At a constant temperature we can use the forward current density J_F as a measure of the generation rate . We found a power-law dependence of EL intensity on J_F, $I_{EL} \propto J_F^{\gamma}$, in a-Si:H p-i-n diodes when the injection current density is larger than 0.5 mA/cm^2. An exponent $\gamma > 1$ at low temperatures and $\gamma \cong 1$ at room temperature was found. Figs. 5a and 5b show the EL intensity as a function of forward current density at several temperatures for the p-i-n and p-i_H-n cells, respectively. There are low- and high- injection regimes in the I_{EL} vs. J_F curves. We have shown, in previous work [11] that when the current density is below 0.5 mA/cm^2, the average separation of the injected carriers is larger than 500 nm, so the tunneling rate would increase with an increase of the carrier density in this nongeminate recombination processes. We pay attention to the high injection regime here. The exponent γ as a function of temperature is plotted in Fig. 6 for both the p-i-n and p-i_H-n cells. One finds that the γ value follows the same line in the whole temperature region in these two types of cells. This implies that the recombination mechanism has not been changed by H-dilution.

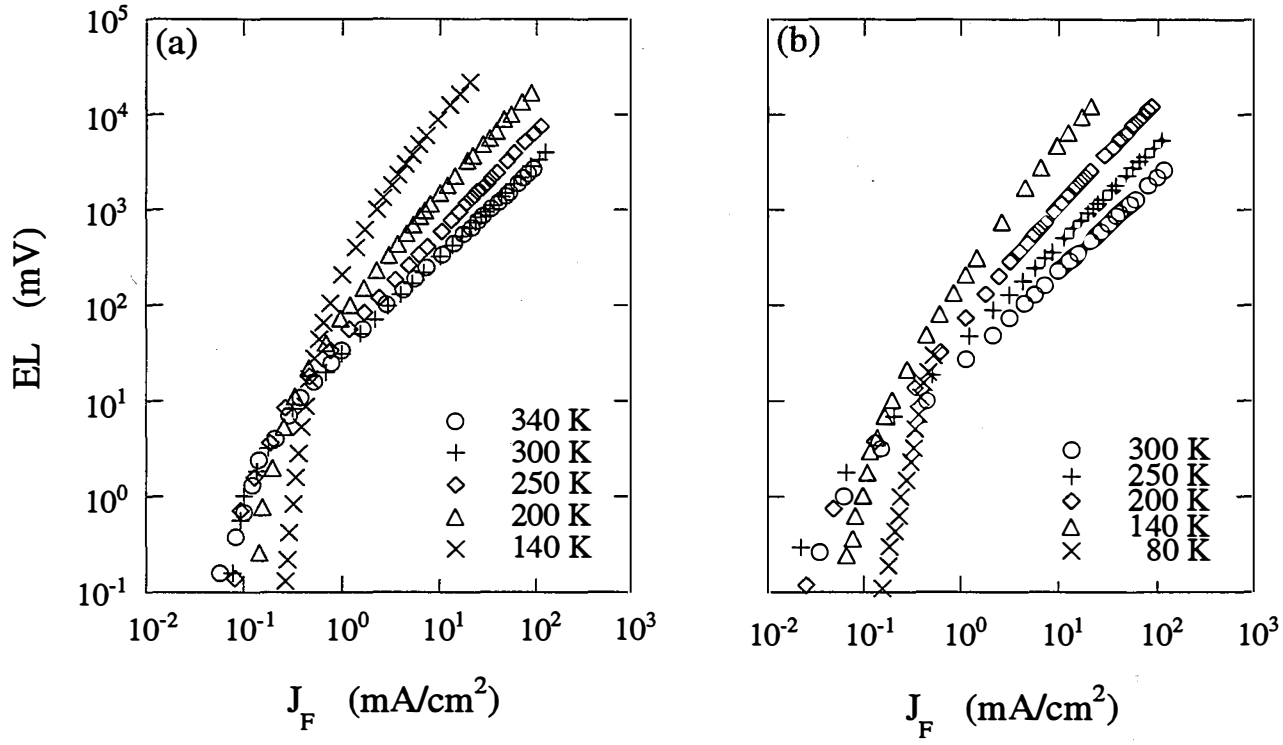

Fig. 5 The EL intensity I_{EL} as a function of forward current density at several temperatures for (a) p-i_H-n , and (b) p-i-n cell.

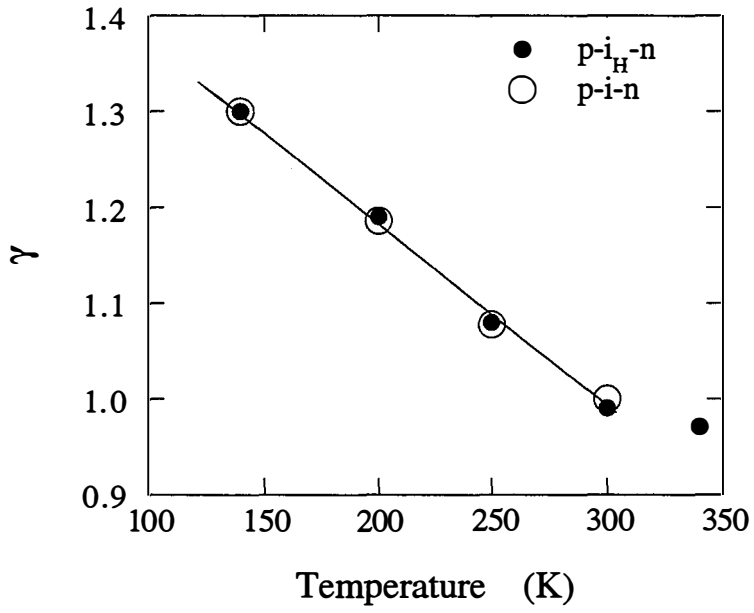

Fig. 6 The exponent γ in $I_{EL} \propto J_F^{\gamma}$ as a function of temperature for the p-i_H-n and p-i-n cell.

EL spectra from p-i-n and p-i_H-n cells

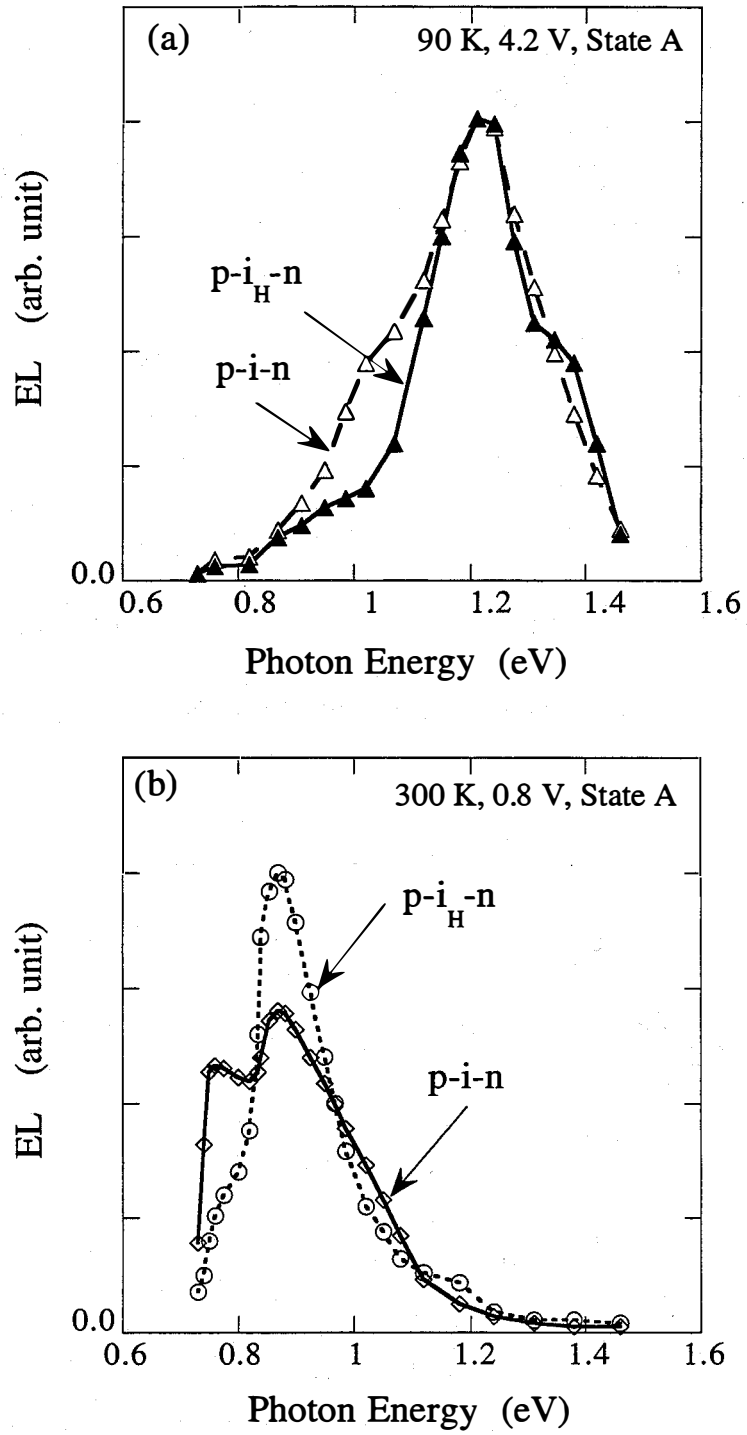

Fig. 7 EL spectra of a-Si:H p-i-n cells made with and without H-dilution in the initial state A (a) at 90 K under 4.2 V, and (b) at 300 K under 0.8 V.

One used to see a featureless photoluminescence band from a-Si:H films.[9] A featureless PL band has also been observed in these p-i_H-n and p-i-n cells.[12] However, the EL spectrum lineshape has shown features in thin a-Si:H p-i-n cells. Figs. 7a and 7b show the EL spectra for the same group of cells as in Figs. 3-6 measured at 90 K with 4.2 V, and 300 K with 0.8 V bias voltage at initial state A, respectively. We observed the main-band luminescence domination at 90 K and the defect band domination at room temperature. In order to compare the lineshape, the spectra were normalized to the same height in Fig. 7a. It is clear that the EL main band from tail-to-tail transition shows a narrower shoulder in the low energy side in the p-i_H-n cell than that in the p-i-n cell. If the EL band width is due to the energy distribution of band tail states,[9] the results indicate a narrower band tail in the p-i_H-n cell than that in the p-i-n call. This is consistent with the above results in Figs. 4a and 4b that show a narrower valence band tail in the hydrogen-diluted cell. More interestingly, in Fig. 7b the defect band for the cell made with H-dilution is dominated by a single peak at ~ 0.9 eV and the cell made without H-dilution has a much more pronounced second peak at ~0.75 eV. Even though the line shape at the low energy side below 0.7 eV is uncertain because of the cut-off energy of the Ge detector, the double-peak feature in the non-diluted cell is clear. It is understandable that during the i-layer growth the hydrogen-diluted reaction gas with slow growth rate gives more chance to form strong Si-H bonds by breaking the weak Si-Si bonds. As a consequence, a narrower band tail, in other words, a larger band gap is obtained in H-diluted cells. This could result in a slightly larger V_{oc} in the solar cell performance. On the other hand, the elimination of the ~0.75 eV low energy defect states by H-dilution can be due to the improvement of the quality of the interface region near p/i junction. This is crucial for the improvement of the stability because of the ~ 0.75 eV defect related with the "slow" metastable defect in the cell.[4,5] We have found[13] that the near interface region dominates the defect luminescence.

Light-induced effects on EL defect-band

In order to find the role of hydrogen dilution in metastability of a-Si:H solar cells, we emphasize the studies of EL in a-Si:H p-i-n solar cells made with hydrogen dilution in comparison with that without hydrogen dilution. The photodegradation kinetics of the forward current and EL were measured up to 1000 h light-soaking under AM1.5 light.

As we know that the defect-band luminescence domination at room temperature, especially at low applied field, that provides direct information on the defect energy profile as discussed above. It is very interesting to study the evolution of the defect properties as the material is being light-soaked. We have exposed both types of cells to 200 mW/cm^2 white light through the p-layer. The light-soaking condition used was similar to the performance photodegradation studies of the same types of solar cells.[4,5] All the parameters of J_F, I_{EL}/I_F and the EL spectrum were measured following step-by-step light soaking. We found slight changes in J_F, I_{EL}/I_F data but clear changes in EL defect spectrum. In Fig. 8 we show EL_d spectra at 0.8 V, 300 K, at various stages of light-soaking for the cell made without H-dilution. The right side figure is the enlarged part of the defect band. As the solar cells are being light-soaked, the intensity of the EL main-band (1.1-1.2 eV) decreases and that of the defect-band increases due to the increase of the density of defect states. The ~0.75 eV defect band continues to grow after the ~0.9 eV band saturated. One can see clearly that the EL_d lineshape changes with prolonged light-soaking.

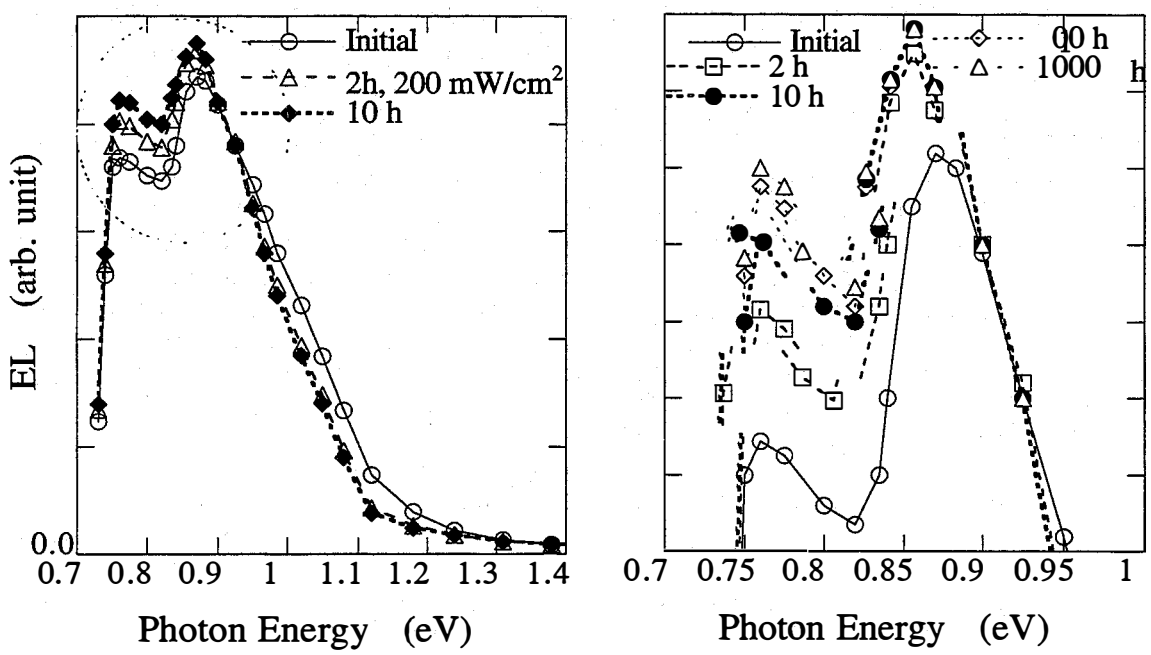

Fig. 8 EL spectra of cells made without H-dilution under 0.8 V at 300 K at various stages of light-soaking. The right side figure is a enlarged part of the defect band.

To investigate the creation kinetics for individual components in the defect band, we have analyzed the intensities of the two peaks at ~0.9 eV and ~0.75 eV, respectively. The results are plotted in Figs.9a and 9b for cells made with and without hydrogen-dilution, respectively. As shown in Fig. 9a, the intensity of the dominant peak at 0.9 eV for the p-i_H-n cell increases first, but rapidly stabilizes after only ~10 hours of light-soaking. No significant change in the low-energy shoulder can be resolved for this type of cell. In contrast, for the non-diluted p-i-n cell as shown in Fig. 9b, the peak at 0.75 eV is much more pronounced and the intensity for both components increases significantly with light-soaking. More interestingly, while the 0.9 eV peak also stabilizes after 10-100 hours of light-soaking, the 0.75 eV peak continues to rise and no sign of saturation is seen even beyond 1000 hours of light-soaking. These observations for both types of cells could be entirely consistent with the results of the solar cell degradation studies [5,6] if we assume that the 0.9 eV and 0.75 eV peaks in the defect band are associated respectively with the "fast" and "slow" defects identified from cell degradation kinetics. Thus, the EL measurements have not only confirmed the existence of the two kinetically different defect states in certain a-Si:H, depending on the deposition condition, but also provided their unique energy characteristics in the electronic energy bandgap.

Considering the defect spectrum $EL_d(h\nu)$ from both the p-i-n and p-i_H-n cells contains two components peaked at 0.9 eV and 0.75 eV, respectively. In Fig. 9 we show the intensities of these defect luminescence components at ~0.9 eV and ~0.75 eV as a function of light-soaking time for (a) p-i_H-n and (b) p-i-n cell. The defect-band ~0.75 eV in the p-i_H-n cell is very weak as shown in Fig.7, the light-induced change is unresolved. Therefore, only the ~0.9 eV band is shown in Fig. 9a for the p-i_H-n cell.

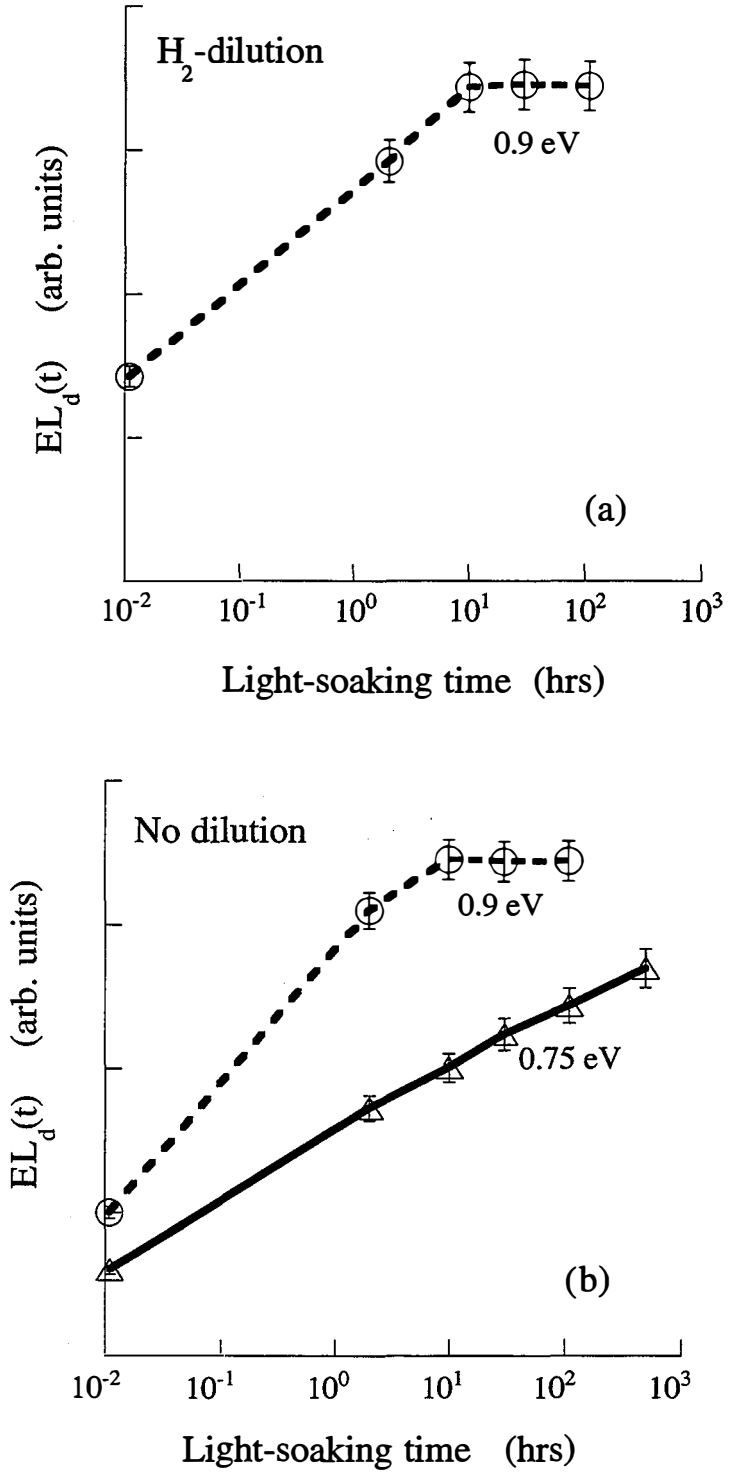

Fig. 9 EL intensities of defect components at ~0.9 eV and ~0.75 eV as a function of light-soaking time for (a) p-i_H-n and (b) p-i-n cell.

I. 4 Conclusions

The main conclusions that we draw from these EL studies are:

(1) We observed that the carrier recombination mechanism in the i-layer has not been changed by hydrogen-dilution in a-Si:H p-i_H-n solar cells, while the band tail width is narrowed and the ~0.75 eV defect luminescence is eliminated by hydrogen-dilution. The slope of the EL efficiency vs. T curve was 29 K, and the defect luminescence band was dominated by a single peak at ~ 0.9 eV for the cell made with H-dilution; while a slope of 37 K, and a dual-peak defect band at ~ 0.9 eV and ~ 0.75 eV were observed for the cell made without H-dilution. We have demonstrated that the results from EL measurements correlate well with the solar cell parameters. The present study confirmed the existence of the "fast" and "slow" defects in a-Si:H and identified their energy positions within the bandgap as a ~0.9 eV and a ~0.75 eV defect band. Our results also reinforced the notion that H-dilution eliminates the microstructure which causes the creation of "slow" defects and hence stabilizes rapidly under light illumination.

(2) The photodegradation kinetics of the defect band suggests that the~0.9 eV and the ~0.75 eV defect band in the EL spectra are actually those identified independently as "fast" and "slow" defects, respectively, from photodegradation studies of solar cells prepared under the same conditions.

(3) Our results indicate that not only the total density but also the energy distribution of the defects are crucial in determining the optoelectronic properties including the stability of amorphous silicon based materials. We have found that the energy profile of the defects depends on fabrication. Therefore, the reproducible results in this work do not mean that the EL spectrum lineshape from a-Si:H p-i-n cells made at the other factories will be the same as in this report, even though both the materials may have the same total density of defect states.

(4) We conclude that EL is a more sensitive tool to study recombination and localized states in a-Si:H p-i-n solar cells. EL measurements appear to form a complement to the existing CPM and PDS techniques to characterize the quality of the intrinsic material (i-layer) and of the correlated p-i-n cells.

II. Transient photocurrents (TPC)

II.1 Introduction

To clarify the correlation of the EL defect band to the deep state energy profile, post-transit photocurrent experiments[14] were carried out in several groups of cells in which the lineshapes of the $EL_d(E)$ were different. The transient photocurrent in the post-TOF time regime, I(t), is electron-emission limited, and the energy profile of the deep states, $N_d(E)$, can be obtained from I(t)t. More detail analysis can be found in the attached paper.[15] The absolute value of $N_d(E)$ needs to be analyzed more carefully but the profile is assured.

II.2 Defect energy profile deduces from TPC in p-i-n solar cells

We have found a good correlation between $EL_d(E)$ and $N_d(E)$ profiles. Fig. 10 shows the small-signal post-transit current results from the same p-i_H-n and p-i-n cells as in Fig. 7b. Comparing the results in Figs. 7b and 10, we conclude first, there is a single-peak band in the p-i_H-n cell and a dual-peak band in the p-i-n cell; second, the features of the energy band are in a mirror symmetry with the $EL_d(E)$ and $N_d(E)$ profiles. This can be understood as the transition path corresponding to EL_d is the transition between the valence band tail and the DBs but the $N_d(E)$ profiles are due to the electron thermal emission from the DBs to the conduction band edge.

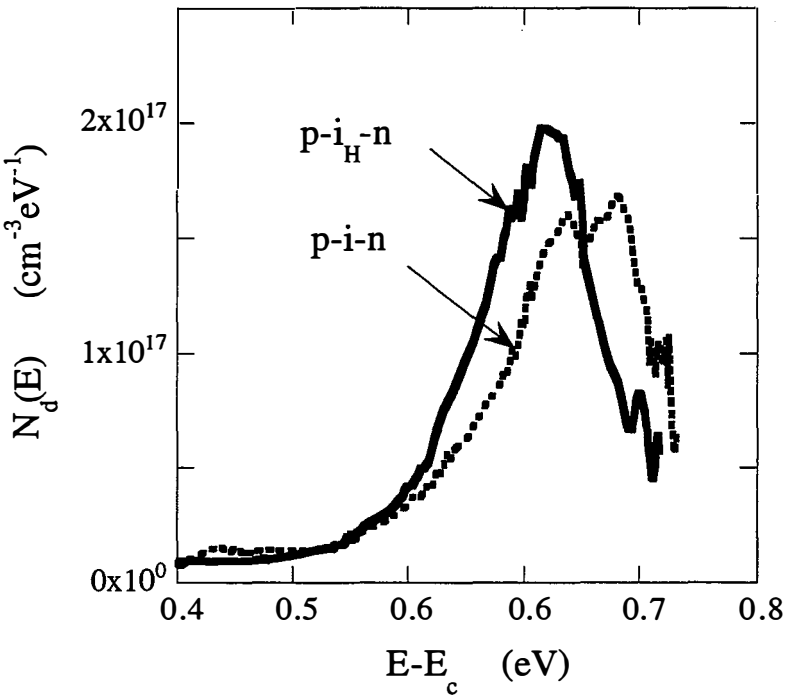

Fig. 10 The small-signal post-transit current results at room temperature from the same p-i_H-n and p-i-n cells as in Fig. 7.

A correlation between the DOS profile from post-transit current measurements[15] and the defect EL spectrum was found as shown in Figs. 7b and 8. This confirms the correlation of room temperature EL spectrum and the defect energy profile, such as the defect band is dominated by a single peak at ~ 0.9 eV for the cell made with H-dilution, while a dual-peak defect band at ~0.9 eV and ~0.75 eV above the valence band edge for the cell made without H-dilution.

I.I 3 Conclusions

The main conclusions from these comparison studies of EL spectrum and post-TOF are:

(1) The lineshape of the EL defect band measured at room temperature reflects the defect energy profile of the i-layer in p-i-n cells.

(2) The low energy luminescence transition path in high quality intrinsic a-Si:H materials is clarified by our EL/post-TOF studies. It is the transition between the valence band tail to the defect states.

III. Internal electric field distribution in p-i-n cells

III.1 Null-current method

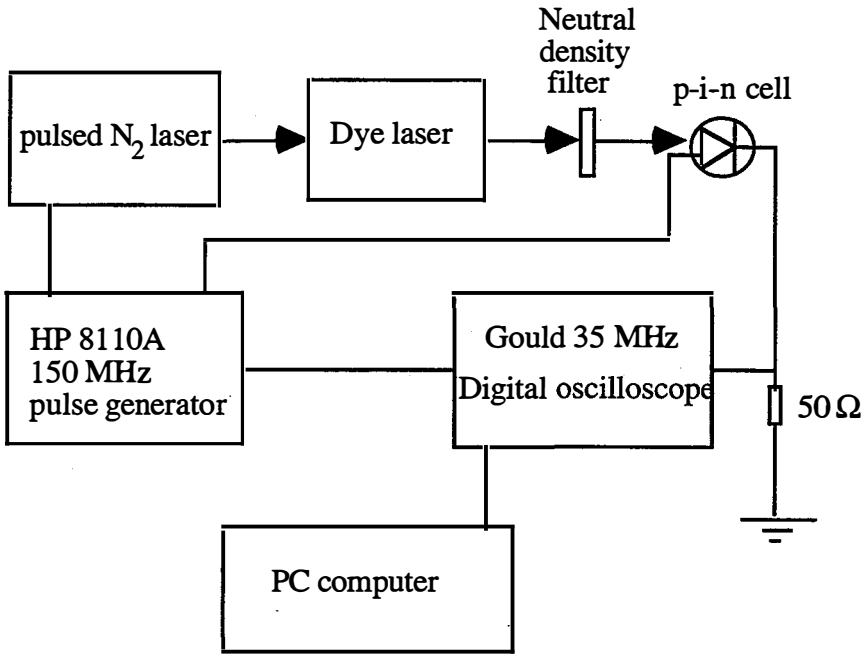

Fig. 11 Block diagram of the transient-null-current experimental apparatus.

Internal electric field distribution is an important parameter for the solar cell design. One needs to know what is the electric field distribution which affects the quantum efficiency wavelength dependence. It is also important to determine how the electric field changes upon light-soaking. We studied the internal electric field profile in p-i-n solar cells by using a transient-null-current method. According to a early demonstration of a null-current technique in a-Si alloy Schottky barrier,[16] the transient photocurrents generated by a low-intensity pulsed laser at a various wavelengths were tuned to zero by the forward-bias voltages and consequently the internal electric field profile can be determined. In the simplest case where the reflection of light is neglected, the photogenerated electron-hole pair density n(x) is given by

$$n(x) = \alpha(\lambda) e^{-\alpha(\lambda)x} I_o t_{pl} , \qquad (3.1)$$

where $\alpha(\lambda)e^{-\alpha(\lambda)x} I_o$ is the generation rate, $\alpha(\lambda)$ is the absorption coefficient, I_o is the incident photon flux of wavelength λ, x is the distance from the p/i interface of the cell, and t_{pl} is the laser pulse width which is less than the carrier's lifetime. Since the p-layer is a wide-gap window, one accounts the distance x from the p-i interface. The photogenerated electron-hole pairs will be separated then swept out by the internal electric field $E_i(x)$ to result in a negative transient photocurrent j_{pc}. The photogenerated peak current just after the excitation is

$$j_{pc} = q\frac{(\mu_n+\mu_p)}{L}\int_o^L [n(x)E_i(x)]dx, \qquad (3.2)$$

where q is the electronic charge, L is the i-layer thickness, and μ_n, μ_p are the drift mobilities for electron and hole, respectively. Since the hole drift mobility in a-Si:H is much less than that of electron's, the contribution of holes to the transient current can be neglected. One applies a positive voltage pulse, V_a, whose amplitude is adjusted until there is no current due to the laser light, e.g.

$$j_{pc} \propto \int_o^L [E_i(x) - V_a/L]e^{-\alpha(\lambda)x}\,dx = 0. \qquad (3.3)$$

Then, V_a at null-current condition can be measured as a function of wavelength λ. One can see in Eq. 3, that the incident photon flux I_o has no direct influence to the value of $E_i(x)$. Realistically, an increase of the incident photon flux would change the space-charge distribution (maybe also the drif mobility) and results in a change of $E_i(x)$. Typically we used a low excitation level to deduce $E_i(x)$. The field profile $E_i(x)$ then can be found by the best fit to the experimental data according to Eq.(3.3) with a specific absorption coefficient $\alpha(\lambda)$.

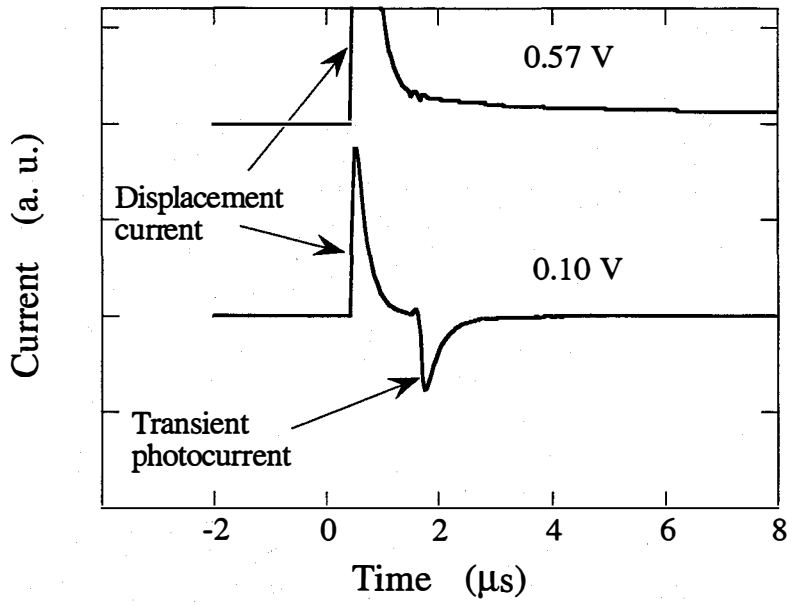

Fig. 12 Measured currents under applied voltage pulses of 0.1 V and 0.57 V for laser pulse at λ = 630 nm for 0.5 μm p-i-n cell.

A dye laser pumped by a pulsed N_2 laser was used for the photo-excitation. The width of the laser pulse t_{pl} is 2×10^{-10} sec, and the wavelength was in the range of 380 - 640 nm. Neutral

density filters were used to adjust the incident light flux. The solar cells were illuminated through the p-layer. A HP 8110A 150 MHz pulse generator with 1×10^{-11} sec resolution was used to apply a positive voltage pulse with 10 μs width. The trigger times of the laser pulse and the voltage pulse can be adjusted separately. The measurements were made at room temperature. A schematic diagram of the experimental apparatus is shown in Fig. 11. To demonstrate the transient-null-current- measurements, the currents at 0.1 V and 0.57 V applied voltage pulses and laser pulse at λ=630 nm for the p-i-n cell are shown in Fig. 12.

In the i-layer, the space-charge density is predominantly determined by trapped carriers in the high concentration of localized states. In order to obtain a reliable value of the internal-electric field, we consider two critical conditions in this transient-null-current technique. (a) To avoid the complicated carrier transport processes, such as deep-trapping, recombination, to disturb the internal-electric-field and the transient current value, we measure the photo carriers which are separated and swept out immediately by the internal-field. Hence, the time window can be used after the displacement current (less than 1 μs in our experiments), and before the rise of the forward-bias recombination current (6-10 μs in our cells depending on applied voltage). The shorter the delay of the laser pulse from the leading edge of the voltage pulse, the more accurate the field strength can be observed. A 1 μs delay was used in this work. (b) To limit the effect of photocarriers on space-charge distribution, the total charge collected was 10^{-10} C per pulse, and a repetition rate 1 Hz was used to ensure that the diode remained close to its equilibrium state. Typically, a signal was averaged 128 times for each wavelength. The experimental error was $\pm$0.05 V.

III.2 Conclusions

During phase II of the subcontract we have completed the set-up and demonstrated that the internal-electric field profile of a-Si:H p-i-n structures can be measured by the transient-null-current method.

We have just started to collaborate with Qi Wang and Crandall at NREL to investigate the internal electric field profile on p-i interface hydrogen-diluted, p-i_H-i-n, solar cells which show a stable V_{oc} upon light-soaking.

The transient-null current method works in the single carrier-space-charge limitation time regime. This method is suitable for both Schottky structure or a p-i-n structure with a longer delay of the recombination current than its RC constant time. Since the recombination current rise time is as short as a few μs in a 0.4-0.5 μm thick p-i-n cells, it is rather difficult to measure the signal precisely. One should use either a Schottky structure or a 0.001 -0.002 cm^2 small dot of a p-i-n structure.

IV. New material studied by Nuclear Magnetic Resonance (NMR)

IV.1 Introduction

From the material point of view, intrinsic a-Si:H deposited by the hot-wire (HW) CVD technique[17] has shown a significant reduction in the generation of light induced defects compared to the standard device-quality PECVD a-Si:H. This material has been produced with a wide range of H contents, but the low H content samples (2-3 at.%) have shown the best electronic properties and the highest stability.[17] Presently, there exists no universally accepted model for SWE.[2] However, most agree that H is involved in some way.[2,3] Although some correlation between the amount of H-related microstructure and the metastability has been suggested, some high quality plasma-enhanced CVD (PECVD) materials do not show detectable microstructures by small-angle x-ray scattering (SAXS), and yet they exhibit SWE.[18] Hence, other experimental methods are needed to examine this question.

We carried out the Nuclear magnetic resonance (NMR) measurements on the low H content, stable HW material. NMR is an ideal method for investigating the H distribution in a-Si:H. Both clustered and isolated phases of H have been identified in device-quality PECVD a-Si:H films that contain 8-10 at.% H.[19,20] On the average, about 70 % of the H is clustered and gives rise to a broad resonance line of 25-33 kHz. Clusters containing 5-7 H atoms have been found using Multiple-Quantum NMR (MQ NMR) in device quality PECVD samples.[21] A narrow peak with a full width at half maximum (FWHM) of a few kHz is also observed in all a-Si:H and is attributed to more dispersed H atoms.[19-21] Attempts have been made to link SWE with this type of local H environment. Preliminary studies of HW suggested a relationship between clustered H and SWE.[22] Other studies have suggested that the isolated H is the most stable and most desirable configuration.[23-25] We address these issues in light of the present NMR results, which are strikingly different from those of any a-Si:H material examined to date.

IV.2 Sample and experimental

Two hot-wire a-Si:H samples were made at NREL by E. Iwaniczko and B. P. Nelson on Al foil wrapped on a stainless steel substrate at 360 °C. No difference in NMR characteristics was found between these two samples. The Al foil was cleaned first using 2% Micro soap in distilled (DI) water using ultrasound, followed by DI water, acetone, and methanol to rinse, and finally isopropanol vapor cleaning and N_2 gas drying. The a-Si:H films were removed by dilute HCl etching and rinsed by DI water, then vacuum-sealed in 4 mm o.d. ESR quartz tubes.

Two aspects of the H microstructures which were investigated in our experiments are the cluster sizes (i.e., the number of H atoms per cluster), estimated by the multiple-quantum NMR (MQ NMR) technique, and the separation distance of neighboring H atoms, based on intrinsic linewidth measurements and MQ NMR. A home-built, low ^1H background NMR probe was used for all NMR measurements. Except for a few spectra taken with a Bruker spectrometer at 4.7 Tesla, all NMR results were obtained using a Chemagnetics spectrometer at 9.4 Tesla. The applied field varied less than 0.05 ppm over the sample volume.

IV. 3 Experimental results

IR ABSORPTION SPECTRUM

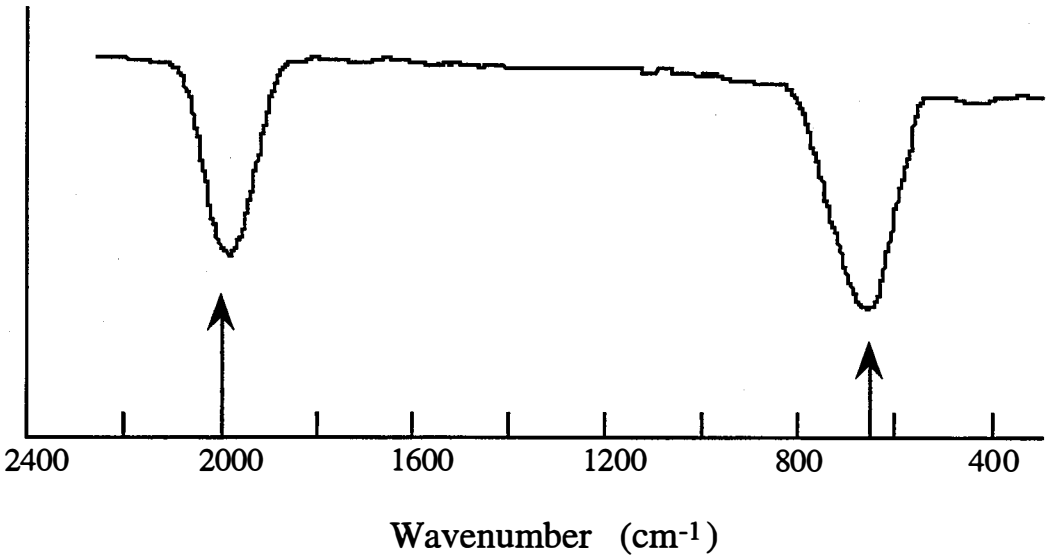

Fig. 13 Typical IR absorption spectrum from hot-wire a-Si:H films with 2-3 at.% H.

The IR spectrum of the HW sample consists of two peaks, one at 630 and the other at 2000 cm^{-1}. It is well-established that this is the signature of the Si-H bonding configuration.[26] A typical HW sample IR curve is shown in Fig. 13. This measurement is significant since it demonstrates that the clustered H responsible for the broad component of the NMR absorption spectrum, shown in Fig. 2(a), must occur as monohydride clusters.

NMR ABSORPTION SPECTRUM AND HOLE BURNING

The free-induction decay (FID) is the NMR signal generated by a single strong radiofrequency (rf) pulse. This pulse provides uniform excitation over the entire spectral width. The Fourier transform of this signal reveals the NMR absorption spectrum for the spin system. Fig. 14(a) shows that the NMR absorption spectrum for the HW sample has a narrow component FWHM of 5.7 kHz and a broad component FWHM of 50 kHz. Although the PECVD spectrum also has a two-component structure, the FWHM of the broad component is only 36 kHz. Furthermore, the HW narrow component FWHM decreases to 3.4 kHz when the applied static magnetic field is reduced to 4.7 Tesla. Similar behavior is observed for the PECVD narrow component FWHM, which decreases from 5.6 kHz to 3.9 kHz under the same conditions. The field dependence of the narrow component implies that the chemical shift interaction accounts for part of this linewidth. This hypothesis can be verified as follows.

The technique of hole burning [19] was used to isolate the contribution of the dipole-dipole interaction to the narrow component of the HW spectrum. This is accomplished using a sequence of equally spaced identical rf pulses known as a Dante sequence.[27] If τ is the time between pulses, δ is the time per pulse, and n_p is the number of pulses, then the excitation profile in the frequency domain consists of a set of bands of width $1/T$, spaced by $1/\tau$, with relative intensities modulated by a sinc function envelope having width $1/\delta$ for the principal maximum.

Here, T is the total time for the pulse sequence, equal to $(n_p-1)\tau+n_p\delta$. The effect of this sequence is to suppress the NMR absorption for a selected frequency range by equalizing the populations of the Zeeman eigenstates for the spin system. This leaves a dip, or "hole", in the NMR absorption. The effect is most pronounced when a series of short, low power pulses is used. The width of the hole cannot be less than the excitation width 1/T. Hence, this technique is useful only for spectral features broader than 1/T. When local interactions besides the chemical shift are present, the minimal hole width may exceed 1/T. In this case, the spin system determines the lower limit for hole width. In particular, when both chemical shift and dipole-dipole interactions affect the spin system, the minimal hole width is a measure of the dipolar coupling strength between spins. The parameter values used for the HW hole-burning spectrum shown in Fig. 14(b) were τ = 200 μs, δ = 0.5 μs, and n_p = 80, giving 1/T = 0.063 kHz. The intrinsic hole width is about 0.5 kHz. This represents the contribution of the dipole-dipole coupling to the total linewidth for the narrow component, and confirms that a considerable portion of the linewidth is associated with the chemical shift interaction. Furthermore, the broad component is strongly saturated by the excitation, indicating that the dipole-dipole interaction accounts for the entire linewidth, and corroborating the observation that the broad component linewidth is the same at different applied magnetic fields.

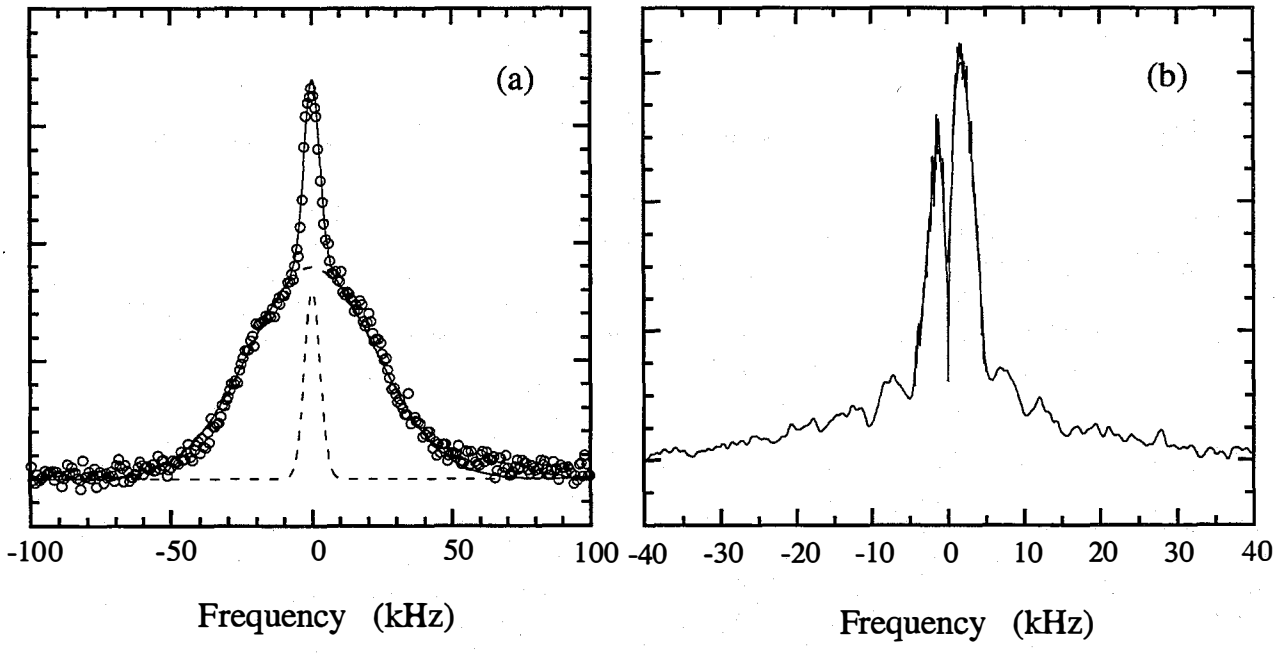

Fig. 14 (a) The ^{1}H NMR spectrum of a high stability HW a-Si:H sample with 2 at.% H, and (b) the hole-burning spectrum of the HW sample. In (a), the open circles are the measured data and the dotted lines are the fitting functions. In (b), the FWHM of the hole is about 0.5 kHz.

MULTIPLE QUANTUM NMR

MQ NMR can be used to determine cluster sizes and interatomic spacing.[21,27] This technique creates multiple-quantum coherences that depend sensitively on the size of the H clusters and the distance between the H atoms in the clusters. These results can be compared with linewidth

measurements. Whereas the effectiveness of hole burning as a frequency-selective technique is limited by the dipolar couplings between spins, these couplings are the basis for the multiple quantum technique. The multiple quantum pulse sequence has no net effect on a spin system without these couplings, since the net spin rotation induced by the pulses is zero. In the presence of the dipole-dipole interaction, however, the effect of these rotations is to develop multiple quantum coherence in a stepwise manner. This is made possible by the internal evolution of the spin system between pulses, which cannot be described in terms of pure rotations of spins. As a result, spin coherences with $|\Delta M| > 1$ are created, even though the selection rule $|DM| = 1$ for magnetic dipole transitions may hold for the individual pulses. (M is the total magnetic quantum number for the spin system). Since M ranges from -N/2 to N/2 for a system of N spin-1/2 particles (e.g., H nuclei), $|\Delta M|$ for pairs of Zeeman eigenstates ranges from 0 to N. Although only $|\Delta M| = 1$ coherences are observable using the NMR detection method, the intensities of higher-order coherences can be determined indirectly using the following method.

The intensities of MQ coherence orders depend on the preparation time τ_p, which was varied by changing the number of cycles l_c of the basic eight 90° pulses in the preparation and mixing periods, as illustrated in Fig. 15. The coherence order intensities are reflected in changes of the FID intensities as a function of the rf phase increment f for the preparation period pulses. In our experiments, f was incremented in 32 steps from 0 to 360°; the typical pulse width was 1 ms; the delay time Δ was 2 ms and the delay time Δ' was $2\Delta+\delta$. Thus, the preparation time per cycle was 36 μs. The entire FID was recorded in the detection period. This allows the determination of MQ spectra associated with both the broad and the narrow component of the FID absorption spectrum. The MQ spectra were determined by taking the Fourier transform with respect to phase of the FID intensities measured at a given decay time for each of the 2 components. Since an even-order selective sequence was employed,[21] the noise level was estimated from the magnitude of the odd-numbered coherence orders.

For a pair of identical spin-1/2 nuclei with gyromagnetic ratio γ, an analytical expression for the normalized MQ signal intensity as a function of ϕ can be derived:

$$\langle I_z \rangle_\phi = \cos^2\phi + \{1 - 2\sin^2[2b_n(3\cos^2\theta - 1)]\} \sin^2\phi , \qquad (4.1)$$

where $$b_n = 2\pi\,(9\times10^4 \text{ rad s}^{-1})\,\Delta'\, n\, (10^{-10} \text{ m}/r)^3\, (\gamma/\gamma_p)^2,$$

r is the internuclear separation, and γ_p is the proton gyromagnetic ratio, equal to $2\pi(4.26\times10^7)$ rad s^{-1} Tesla^{-1}. Here, it is assumed that the internal evolution of the spin system during the individual pulses is negligible. The powder average is proportional to:

$$\langle \langle I_z \rangle_\phi \rangle_{powder} = \cos^2\phi + (1/2)\,(\pi/6b_n)^{1/2} \sin^2\phi \times [\cos(4b_n)\, C(\,2(6b_n/\pi)^{1/2}) + \sin(4b_n) S(2(6b_n/\pi)^{1/2})], \qquad (4.2)$$

where C and S are the Fresnel integral functions. This result is relevant for the interpretation of the narrow component of the FID spectrum. For larger groups of spins, numerical simulations can be performed.

The behavior of the broad component of the NMR absorption spectrum for the HW sample under the sequence in Fig. 15 is shown in Fig. 16 for various preparation times τ_p. The highest-order

coherence continues to increase as τ_p is increased, indicating a large number of strongly dipolar coupled spins. According to the MQ spectrum for the longest τ_p, this number must be at least 14. In contrast, the highest-order coherence developed for the broad component of the PECVD spectrum is DM = 6, even for the longest τ_p . This result suggests that this component is due to isolated clusters containing no more than 7 H atoms each.[21]

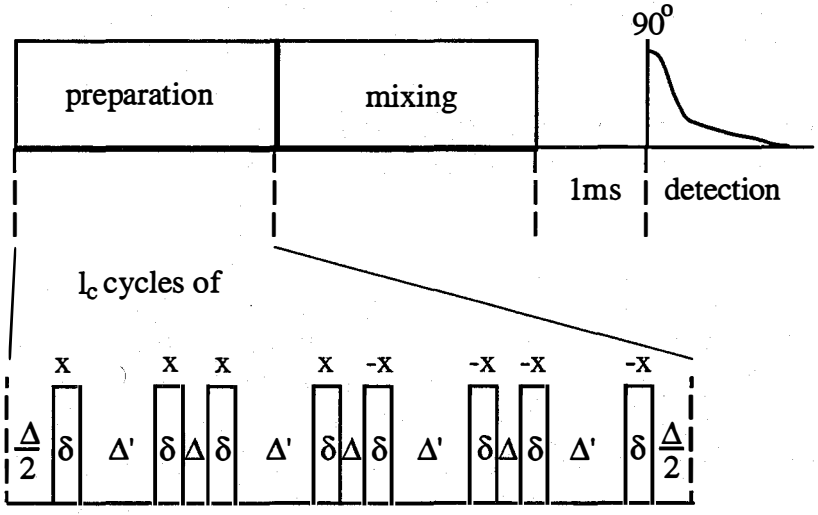

Fig. 15 Pulse sequence for MQ NMR

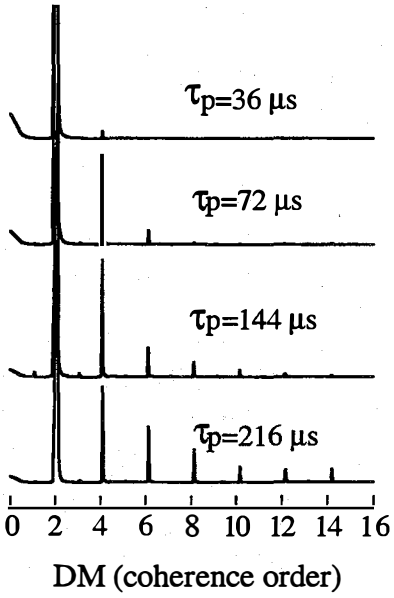

Fig. 16 MQ spectrum for the broad component in the hot-wire sample

IV. 4 Conclusion

The microstructures of 2-3 hydrogen at.% hot-wire CVD a-Si:H films were characterized by ^{1}H Nuclear Magnetic Resonance. Significant differences were found between the hydrogen distribution in these samples and that in conventional plasma-enhanced CVD samples. Among other things, the broad resonance line in the hot-wire a-Si:H is 50 kHz wide, which is much broader than that observed 25-35 kHz in PECVD a-Si:H films. Moreover, a 0.5 kHz resonance absorption hole width due to intrinsic dipolar interactions is obtained using the hole-burning technique. Surprisingly, approximately 90 percent of the hydrogen atoms give rise to the 50 kHz line and only a very small percentage of the hydrogen atoms give rise to the much narrower resonance line.

This result demonstrates very clearly that small H clusters with large numbers of H atoms are the typical microstructure of the high stability HW a-Si:H materials. However, the nature of these H clusters needs to be clarified.

Our MQ NMR results, together with previous works, show that the clusters contain no more than 7 H atoms in PECVD a-Si:H, whereas much larger H complexes occur in HW a-Si:H. These results indicate that multi-vacancy "defects" may be present in HW a-Si:H and these "defects" play an essential role in the relaxation of the a-Si:H network.

Further effort

We have completed the Phase II of the research program and met the project goal. This has been accomplished by the EL spectroscopy and the transient current technique. In addition, we have found the unexpected hydrogen distribution of the hot-wire materials by NMR and MQ NMR techniques without financial support from NREL/DOE. Efforts will be continued to cooperate with team members, especially members from the PV industry to study the factors governing the SWE in a-Si:H solar cells. We will pay more attention to the EL measurements, which give more directly useful information to this subject, and to the internal electric field profile of p-i-n structures. The NMR measurements, which give structural information on the new hot-wire materials are important. We would like to continue the work if we can find financial support.

Publications:

1. Daxing Han and Keda Wang, "A distinct recombination regime in amorphous silicon diodes under double injection", *Appl. Phys. Lett.* **66**, 879-881 (1995).
2. Daxing Han and Keda Wang, "Electroluminescence from hydrogenated amorphous silicon p-i-n diodes" *J. Non-Cryst. Sol.* **190**, 74-84(1995).
3. Regis Vanderhaghen and Daxing Han, "Interface effects on double injection current and photocurrent in a-Si:H n-i-p and p-i-n diodes", *J. Non-Cryst. Sol.***190**, 95-105 (1995).
4. B. Yan, G.J. Adrianenssens, A. Eliat, and D. Han, "Forward current transients in amorphous silicon p-i-n structures", *J. Non-Cryst. Sol.* **190**, 85-94 (1995).
5. Keda Wang and Daxing Han, "Relation of the EL measurements to solar cell parameters", in *Amorphous Silicon Technology*, edited by E.A. Schiff, M. Hack, A. Madam, M. Powell, A. Matsuda, MRS Symp. Proc.**377** (1995) 633.
6. C.N. Yeh, D.X. Han, K.D. Wang and L.E. McNeil, "Carrier recombination in a-Si:H p-i-n devices studied by PL and EL spectroscopies", in *Amorphous Silicon Technology,* edited by E.A. Schiff, M. Hack, A. Madan, M. Powell, A. Matsude, MRS Symp. Proc.**377** (1995) 281.
7. Baojie Yan, Daxing Han, and G.J. Adrianenssens, "Analysis of post-transit photocurrents and electroluminescence spectra from a-Si:H solar cells", J. Appl. Phys. **79** (1996) 3597.
8. Chen-Nan Yeh, Qi Wang, and Daxing Han, "The effect of hydrogen dilution near the p/i interface region on DOS profile in a-Si:H p-i-n solar cells", to be published in Amorphous Silicon Technology-1996, edited by M. Hack, E. A. Schiff, M. Powell, A. Matsuda, and A. Madan (MRS Symposium Proceedings, San Francisco, CA, 1996).
9. J. Todd. Stephen, Daxing Han, Harv Mahan, and Yue Wu, "Hydrogen distribution in high stability a-SI:H prepared by the hot wire technique", ibid.
10. Daxing Han, Keda Wang, and Liyou Yang, "Recombonation and metastability of amorphous silicon solar cells made with and without hydrogen dilution studied by Electroluminescence spectroscopy", to be published in J. Appl. Phys. 96.8.
11. Y. Wu, J. Todd. Stephen, Daxing Han, Harv Mahan, and R. A. Crandall, "Hydrogen distribution in hot wire a-SI:H" to be published in PRL. 96.9

References

1. D.L. Staebler and C.R.Wronski, Appl. Phys. Lett. **31**, 292 (1977).
2. H. Fritzsche, J. Non-Cryst. Sol. **190,** 180 (1995).
3. 9. M. Stutzmann, W. B. Jackson, and C. C. Tsai, Phys. Rev. B **32**, 23 (1985).
4. L. Yang and L. Chen, Appl. Phys. Lett. **63** (1993) 400.
5. L. Yang and L. Chen in "Amorphous Silicon Technology," edited by E. A. Schiff, M.Hack, A. Madan, M. Powell, A. Matsuda, (MRS Symp. Proc. **336** 1994) pp. 669-674.
6. "Research on Stable, High-Efficiency Amorphous Silicon Multijunction Modules", NREL Final Subcontract Report, 1 Jan. 91-31 Aug. 94, USSC, p.34
7. Daxing Han and Keda Wang, J. Non-Cryst. Sol. **190**, 74 (1995).
8. R. W. Collins, M. R. Paesler, and W. Paul, Solid State Commun. **34**, 833 (1980); R. W. Collins and W. Paul, Phys. Rev. **B25**, 5257 (1982).
9. R. A. Street, in "Semiconductors and Semimetals", Vol 21B, edited by J.I. Pankove, Academic Press, Inc, 1984) p.199.
10. Keda Wang, Daxing Han, and M. Silver, in *Amorphous Silicon Technology*, edited by E. A. Schiff, M.Hack, A. Madan, M. Powell, A. Matsuda, MRS Symp. Proc. **336** 861-866 (1994).
11. Daxing Han and Keda Wang, *Appl. Phys. Lett*. **66**, 879-881 (1995).
12. C.N. Yeh, D.X. Han, K.D. Wang and L.E. McNeil, in *Amorphous Silicon Technology,* edited by E.A. Schiff, M. Hack, A. Madan, M. Powell, A. Matsude, MRS Symp. Proc. **377** (1995) 281.
13. Keda Wang, Daxing Han, and M. Silver, in *Amorphous Silicon Technology,* edited by E.A. Schiff, M. Hack, A. Madan, M. Powell, A. Matsude, MRS Symp. Proc. **297** 857-862 (1993).
14. G. F. Senhaeve, R. P. Barclay, G. J. Adriaenssens, and J. M. Marshall, Phys. Rev. B **39** 10196 (1989).
15. Baojie Yan, Daxing Han, and G.J. Adrianenssens, "Analysis of post-transit photocurrents and electroluminescence spectra from a-Si:H solar cells", J. Appl. Phys. **79**, 3597 (1996).
16. T. Datta and M. Silver, Appl. Phys. Lett. 38, 903 (1981).
17. A. H. Mahan, J. Carapella, B. P. Nelson, R. S. Crandall, and I. Balberg, J. Appl. Phys. **69**, 6728 (1991).
18. D. L. Williamson, in *Amorphous Silicon Technology*, edited by E. A. Schiff, M.Hack, A. Madan, M. Powell, A. Matsuda, (MRS Symp. Proc. **377**, 1995), pp. 251-262.
19. J. A. Reimer and M. A. Petrich, in *Amorphous Silicon and Related Materials*, edited by H. Fritzsche (World Scientific Co. Singapore, 1989), pp. 3-27.
20. P.C. Taylor, in *Semiconductors and Semimetals*, vol. **21**C Hydrogenated Amorphous Silicon, edited by J. I. Pankove (Academic Press, Inc. 1984), p. 99.
21. J. Baum, K. K. Gleason, A. Pines, A. N. Garroway, and J. A. Reimer, Phys. Rev. Lett. **56**, 1377 (1986); K. K. Gleason, M. A. Petrich, and J. A. Reimer, *Phys. Rev. B* **36**, 3259 (1987).
22. M. Vanecek, A. H. Mahan, B. P. Nelson,, and R. S. Crandall, Proc. 12th Europ. PV Solar Energy Conference, (April 1994, Amstedam, the Netherlands), p.354.
23. J. A. Reimer and Robet W. Vaughan, Solid State Commun. **37** 161 (1981).
24. W. Beyer and H. Wagner, J. Non-Cryst. Sol. **59/60,** 161 (1983).
25. T. Shimizu, K. Nakazawa, M. Kumeda, and S. Ueda, Japanese J. Appl. Phys., **21**, L351 (1982); T. Shimizu, J. Non-Cryst. Sol. **59/60,** 117 (1983); M. Kumeda, H. Komatsu, T. Shimizu, N. Fukuda and N. Kitagawa, Jpn. J. Appl. Phys. **24**, L495 (1985).
26. G. Lucovsky, R. J. Nemanich, and J. C. Knights, Phys. Rev. B **19**, 2064 (1979).
27. R. Freeman, *A Handbook of Nuclear Magnetic Resonance*, (Longman Scientific & Technical, Essex, UK, 1988), p. 207.

REPORT DOCUMENTATION PAGE

Form Approved
OMB NO. 0704-0188

1. AGENCY USE ONLY (Leave blank)	2. REPORT DATE	3. REPORT TYPE AND DATES COVERED
	October 1996	Annual Subcontract Report, 1 April 1995 - 30 June 1996

4. TITLE AND SUBTITLE

Experimental Study of the Factors Governing the Staebler-Wronski Photodegradation Effect in a-Si:H Solar Cells; Annual Subcontract Report, 1 April 1995 - 30 June 1996

5. FUNDING NUMBERS

C: XAN-4-13318-09
TA: PV631101

6. AUTHOR(S)

D. Han

7. PERFORMING ORGANIZATION NAME(S) AND ADDRESS(ES)

University of North Carolina
Chapel Hill, North Carolina

8. PERFORMING ORGANIZATION REPORT NUMBER

9. SPONSORING/MONITORING AGENCY NAME(S) AND ADDRESS(ES)

National Renewable Energy Laboratory
1617 Cole Blvd.
Golden, CO 80401-3393

10. SPONSORING/MONITORING AGENCY REPORT NUMBER

SR-520-21928

DE96014326

11. SUPPLEMENTARY NOTES

NREL Technical Monitor: B. von Roedern

12a. DISTRIBUTION/AVAILABILITY STATEMENT

12b. DISTRIBUTION CODE

UC-1262

13. ABSTRACT *(Maximum 200 words)*

This report describes continuing experiments on electroluminescence (EL), field profile, and H-microstructure studies of a-Si:H-based solar cells and materials. By using EL spectroscopy, we observed that both the band-tail width and the defect energy distribution are narrowed by H-dilution. We demonstrated the existence of the "fast" and "slow" defects in the cell performance and identified their energy positions as a ~0.9 eV and a ~0.75 eV defect EL band. Our results also reinforced the notion that H-dilution eliminates the microstructure that causes the creation of "slow" defects and hence stabilizes rapidly under light illumination. We demonstrated that the internal-electric field profile of a-Si:H p-i-n structures can be measured by the transient-null-current method. For the first time, hot-wire-deposited a-Si:H films were characterized by ^{1}H nuclear magnetic resonance. Surprisingly, about 90 percent of the H atoms give rise to the 50-kHz line, and only a very small percentage of the H atoms give rise to the 3-kHz-narrower resonance line, which suggests that H-bonding in hot-wire films is very different from that in a-Si:H produced by plasma-enhanced chemical vapor deposition.

14. SUBJECT TERMS

photovoltaics ; amorphous silicon research ; electroluminescence ; hydrogenated amorphous silicon ; hot-wire films ; Staebler-Wronski Effect

15. NUMBER OF PAGES
34

16. PRICE CODE

17. SECURITY CLASSIFICATION OF REPORT	18. SECURITY CLASSIFICATION OF THIS PAGE	19. SECURITY CLASSIFICATION OF ABSTRACT	20. LIMITATION OF ABSTRACT
Unclassified	Unclassified	Unclassified	UL